Monthly Notices
of the
ROYAL ASTRONOMICAL SOCIETY

MNRAS **462,** 663–680 (2016)
Advance Access publication 2016 July 14

doi:10.1093/mnras/stw1688

NIHAO project II: halo shape, phase-space density and velocity distribution of dark matter in galaxy formation simulations

Iryna Butsky,[1,2,3] Andrea V. Macciò,[1,4★] Aaron A. Dutton,[1,4] Liang Wang,[1,5,6] Aura Obreja,[4] Greg S. Stinson,[1] Camilla Penzo,[1,7] Xi Kang,[5] Ben W. Keller[8] and James Wadsley[8]

[1]*Max-Planck-Institut für Astronomie, Königstuhl 17, D-69117 Heidelberg, Germany*
[2]*University of Washington, Seattle, Washington, WA 9 8195-1580, USA*
[3]*California Institute of Technology, Pasadena, California, CA 91125, USA*
[4]*New York University Abu Dhabi, PO Box 129188, Abu Dhabi, UAE*
[5]*Purple Mountain Observatory, the Partner Group of MPI für Astronomie, 2 West Beijing Road, Nanjing 210008, China*
[6]*Chinese Academy of Science Graduate School, Beijing, China*
[7]*Laboratoire Univers et Théories, UMR 8102 CNRS, Observatoire de Paris, Université Paris Diderot, 5 Place Jules Janssen, F-92190 Meudon, France*
[8]*Department of Physics and Astronomy, McMaster University, Hamilton, Ontario L8S 4M1, Canada*

Accepted 2016 July 12. Received 2016 July 7; in original form 2015 March 19

ABSTRACT

We use the NIHAO (Numerical Investigation of Hundred Astrophysical Objects) cosmological simulations to study the effects of galaxy formation on key properties of dark matter (DM) haloes. NIHAO consists of ≈90 high-resolution smoothed particle hydrodynamics simulations that include (metal-line) cooling, star formation, and feedback from massive stars and supernovae, and cover a wide stellar and halo mass range: $10^6 \lesssim M_*/\mathrm{M}_\odot \lesssim 10^{11}$($10^{9.5} \lesssim M_{\rm halo}/\mathrm{M}_\odot \lesssim 10^{12.5}$). When compared to DM-only simulations, the NIHAO haloes have similar shapes at the virial radius, $R_{\rm vir}$, but are substantially rounder inside $\approx 0.1R_{\rm vir}$. In NIHAO simulations, c/a increases with halo mass and integrated star formation efficiency, reaching ∼0.8 at the Milky Way mass (compared to 0.5 in DM-only), providing a plausible solution to the long-standing conflict between observations and DM-only simulations. The radial profile of the phase-space Q parameter (ρ/σ^3) is best fit with a single power law in DM-only simulations, but shows a flattening within $\approx 0.1R_{\rm vir}$ for NIHAO for total masses $M > 10^{11}\,\mathrm{M}_\odot$. Finally, the global velocity distribution of DM is similar in both DM-only and NIHAO simulations, but in the solar neighbourhood, NIHAO galaxies deviate substantially from Maxwellian. The distribution is more symmetric, roughly Gaussian, with a peak that shifts to higher velocities for Milky Way mass haloes. We provide the distribution parameters which can be used for predictions for direct DM detection experiments. Our results underline the ability of the galaxy formation processes to modify the properties of DM haloes.

Key words: Galaxy: disc – Galaxy: evolution – Galaxy: structure – galaxies: evolution – galaxies: interactions – galaxies: structure – methods: numerical.

1 INTRODUCTION

N-body numerical cosmological simulations have proven to be powerful tools for modelling the properties of the three-dimensional dark matter (DM) distribution in galactic haloes (Jing & Suto 2002; Allgood et al. 2006; Bett et al. 2007; Hayashi, Navarro & Springel 2007; Macciò et al. 2007; Neto et al. 2007). However, these DM-only cosmological simulations only take into account the effects of gravity. Globally, the baryons only make up $\Omega_{\rm b}/\Omega_{\rm m} \approx 15$ per cent of the mass budget (Planck Collaboration XVI 2014), and thus on large scales, their influence can be reasonably ignored. However, baryons can dissipate energy, leading to large-mass fractions near the centres of galaxies. Additional processes such as the violent explosion of stars as supernovae (SNe) can have non-negligible impact on the DM distribution.

Using the Λcold dark matter (CDM) cosmology, DM-only galaxy simulations can make precise predictions of the shape and the internal matter and velocity distribution of DM haloes (Macciò, Dutton & van den Bosch 2008). On average, such dissipationless

★ E-mail: maccio@nyu.edu

cosmological simulations predict the ratio of the minor principal axis to the major to be $\langle c/a \rangle \sim 0.6$. Observations, however, indicate that haloes are more spherical. Ibata et al. (2001) used the Sagittarius Stream (and a Dehnen & Binney 1998 halo mass distribution) to put a lower bound on the shape of the inner Milky Way halo of $c/a \geq 0.8$, where the halo was defined to be in the range 20 kpc $< r <$ 60 kpc. Other recent work found similarly spherical shapes for the inner halo of the Milky Way (Helmi 2004; Martínez-Delgado et al. 2004).

In a recent, detailed study, Law & Majewski (2010) presented a new N-body model (with a logarithm DM halo)[1] for the tidal disruption of the Sagittarius galaxy which led them to conclude that our Galaxy has an oblate potential with a minor to major axis ratio of $(c/a)_\phi = 0.72$. This latter value can be seen as a upper limit on the shape of the matter distribution, which again suggests a possible tension between results of pure CDM simulations and local measurements of halo shape.

One possible solution to this problem could be related to the inclusion of a dissipative component such as baryons in cosmological simulations. Katz & Gunn (1991) and Dubinski (1994) were among the first to show that haloes in dissipative simulations were systematically more spherical than corresponding haloes in dissipationless simulations. Kazantzidis et al. (2004) analysed the effect of baryons on the shape of DM haloes using high-resolution hydrodynamical simulations of clusters of galaxies and, again, found a reduced triaxiality in dissipational simulations. That result was confirmed in several further studies (Springel, White & Hernquist 2004; Debattista et al. 2008; Pedrosa, Tissera & Scannapieco 2009; Tissera et al. 2010). While there is an agreement that baryons tend to make DM haloes rounder, a quantitative prediction of this effect strongly depends on the prescription used to model baryons in cosmological simulations, which is not a trivial task.

A large fraction of simulated galaxies used for studying the impact of baryons on the DM distribution were either plagued by the so-called overcooling problem (which produced galaxies that were unrealistically dominated by baryons in their central region; Kazantzidis et al. 2004) or were missing important aspects of the galaxy formation process, such as star formation and feedback (Abadi et al. 2010).

A noticeable exception has been the recent work by Bryan et al. (2013), which employed the OverWelmingly Large simulations (Schaye et al. 2010), a large-scale simulation that produced realistic large galaxies and cosmic structure in a full cosmological framework. These simulations found that baryons substantially changed c/a of massive galaxies. On the other hand, they were able to resolve galaxies on the scale of the Milky Way with only few thousand particles.

Shape is not the only parameter of DM haloes that baryons might modify. A lot of recent attention has focused on the modification (expansion and core creation) of density profiles (Gnedin et al. 2004; Abadi et al. 2010; Governato et al. 2010; Macciò et al. 2012; Pontzen & Governato 2012; Di Cintio et al. 2014b; Dutton et al. 2015; Oñorbe et al. 2015), which helps reduce the tension on small scales between observations (e.g. Oh et al. 2015, and references therein) and DM-only predictions (Dutton et al. 2016b; Tollet et al. 2016). Another interesting quantity that is a slight variant on the density profile is the so-called coarse-grained phase-space density $Q = \rho/\sigma^3$ that takes into account particle velocities as well as matter density. DM-only simulations show that radial profiles of Q are well fit with a simple power law $\rho/\sigma^3 \propto r^\alpha$ (Taylor & Navarro 2001).

Analytical work found a characteristic value for the power-law slope of the Q profile, $\alpha = 1.944$, for isotropic structures (Austin et al. 2005). This value also reproduces realistic radial velocity dispersions through cosmological simulations (Dehnen & McLaughlin (2005), but see also Schmidt et al. 2008 for a more critical interpretation). It is particularly interesting to check if baryons break this simple power-law behaviour of the DM coarse-grained phase-space density in simulated galaxies.

The DM velocity distribution is another very important parameter, since it has profound implications for the predicted DM–nucleon scattering rates in direct detection experiments (Kuhlen et al. 2010). Most models assume a Maxwell–Boltzmann (MB) velocity distribution function. Therefore, a departure from the MB distribution might change the predicted rate of events for DM models in which the scattering is sensitive to the high-velocity tail of the distribution, and for experiments that require high-energy recoil events (e.g. Vergados, Hansen & Host 2008).

Recent high-resolution DM-only simulations have reported substantial departures from a Maxwellian shape (Vogelsberger et al. 2009; Kuhlen et al. 2010), with a deficit near the peak and excess particles at high speeds. In contrast, an analysis of the ERIS hydrodynamical simulation of a single Milky Way-like galaxy, showed a different behaviour. Its velocity function maintains the Maxwellian distribution and shows a greater deficit than MB at high velocities (Pillepich et al. 2014).

In this paper, we revisit the issues of the effect of baryons on DM properties using the galaxies from the Numerical Investigation of Hundred Astrophysical Objects (NIHAO) project (Wang et al. 2015). The NIHAO project is a large suite of high-resolution simulated galaxies. The sample includes more than 90 high-resolution zoom regions with halo masses ranging from $\sim 10^{10}$ to $\sim 10^{12}$ $M_\odot$. Each high-resolution galaxy is resolved with at least 600 000 elements (DM+GAS) and up to several millions (see Wang et al. 2015 for details). It is the largest sample of high-resolution galaxies to date. The simulations show remarkable agreement with the stellar mass–halo mass relationship across five orders of magnitude of stellar mass. Thus, a fully sampled volume would follow the observed galaxy stellar mass function. The simulations thus offer a unique tool to study the modifications that baryons induce to DM since it simultaneously combines high spatial and mass resolution with a statistical sample of galaxies across three orders of magnitude in halo mass.

We have decided to focus this paper on three main properties: the halo shape, since it is a widely studied halo property and it is possible to directly measure it, especially in our own galaxy, the (pseudo) phase-space density, since it has been claimed to be an universal property of DM haloes (Taylor & Navarro 2001) and it is somehow complementary to the DM density profiles which have been discussed in the NIHAO IV paper, and the DM velocity distribution that has important consequences on the predicted rate of events in direct detection experiments. Another interesting property is the angular momentum distribution of the DM, but this will be the topic of a different NIHAO paper more closely linked to the process of disc formation (Obreja et al., in preparation)

This paper is organized as follows: in Section 2, we discuss the simulations including the feedback prescription used in creating the NIHAO galaxies; In Section 3, we discuss in detail the effects of baryons on the DM halo shape, pseudo phase space density and the velocity distribution. Section 4 offers a summary of our results, as well as their impact.

[1] An NFW profile will give similar results (Law & Majewski 2010).

2 SIMULATIONS

We study simulations from the NIHAO project (Wang et al. 2015), that use baryonic physics from an updated version of the MaGICC simulations (Stinson et al. 2013). The initial conditions are created using the latest compilation of cosmological parameters from the *Planck satellite* (Planck Collaboration XVI 2014); namely $\Omega_\Lambda = 0.6825$, $\Omega_m = 0.3175$, $H_0 = 67.1$, $\sigma_8 = 0.8344$, $n = 0.9624$ and $\Omega_b = 0.0490$. The haloes to be re-simulated with baryons and higher resolution were extracted from three different pure *N*-body simulations with box sizes of 60, 20 and 15 h^{-1} Mpc; more information on the DM-only simulations can be found in Dutton & Macciò (2014).

The NIHAO project was designed to study galaxy formation over a wide mass range, from dwarf galaxies to massive spirals like the Milky Way. The simulations maintain the same numerical resolution across the entire mass range. This means that all haloes are resolved with at least 600 000 elements (DM+stars+GAS) within the virial radius, up to several millions. This fixes numerical resolution has been achieved by varying both the size of the initial box from which the haloes to be zoomed have been chosen, and the number of zoom levels of each simulation (see fig. 2 in Wang et al. 2015).

The zoomed initial conditions were created using a modified version of GRAFIC2 (Bertschinger 2001; Penzo et al. 2014). All haloes/galaxies presented in this paper are the most massive object in their respective high-resolution volume, in other words, we will only present results, at all masses, for central haloes. The starting redshift is $z_{start} = 100$, and each halo is initially simulated at high resolution with DM-only using PKDGRAV (Stadel 2001). More details on the sample selection can be found in Wang et al. (2015).

We refer to simulations with baryons as the hydro simulations or NIHAO, while we will use the term *N*-body or DM-only for the collisionless simulations.

The hydro simulations are evolved using an improved version of the SPH code GASOLINE (Wadsley, Stadel & Quinn 2004). The code includes a subgrid model for turbulent mixing of metals and energy (Wadsley, Veeravalli & Couchman 2008), heating and cooling include photoelectric heating of dust grains, ultraviolet heating and ionization and cooling due to hydrogen, helium and metals (Shen, Wadsley & Stinson 2010).

For the NIHAO simulations, we have used a revised treatment of hydrodynamics described in Keller et al. (2014) that we refer to as ESF-GASOLINE2. Most important is the Ritchie & Thomas (2001) force expression that improves mixing and shortens the destruction time for cold blobs (see Agertz et al. (2007)). ESF-GASOLINE2 also includes the time-step limiter suggested by Saitoh & Makino (2009), which is important in the presence of strong shocks and temperature jumps. We also increased the number of neighbour particles used in the calculation of the smoothed hydrodynamic properties from 32 to 50.

2.1 Star formation and feedback

The star formation and feedback modelling follows what was used in the MaGICC simulations (Stinson et al. 2013). Gas can form stars when it satisfies a temperature and a density threshold: $T < 15\,000$ K and $n_{th} > 10.3$ cm^{-3}. Stars can feed energy back into the interstellar medium (ISM) via blast-wave SN feedback (Stinson et al. 2006) and via ionizing radiation from massive stars before they turn in SN. Metals are produced by Type II SN, Type Ia SN. These, along with stellar winds from asymptotic giant branch stars, also return mass to the ISM. The metals affect the cooling function (Shen et al. 2010) and diffuse between gas particles (Wadsley et al. 2008). The fraction of stellar mass that results in SN and winds is determined using the Chabrier (2003) stellar initial mass function.

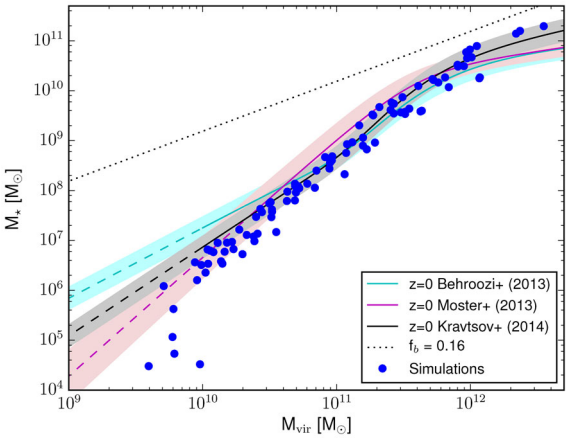

Figure 1. Stellar mass–halo mass relation for the NIHAO galaxies used in this work. All simulations have more than 600 000 particles in their virial radius (see Wang et al. 2015 for more details). The solid lines represent the most commonly used abundance matching results (see the text).

There are two small changes from the MaGICC simulations. The change in number of neighbours and the new combination of softening length and particle mass means the threshold for star formation increased from 9.3 to 10.3 cm^{-3}, The increased hydrodynamic mixing necessitated a small increase of pre-SN feedback efficiency, ϵ_{ESF}, from 0.1 to 0.13. This energy is ejected as thermal energy into the surrounding gas, which does not have its cooling disabled. Most of this energy is instantaneously radiated away, and the effective coupling is of the order of 1 per cent.

2.2 The galaxy sample

For this project, we use a total of 93 galaxies from the NIHAO sample, all galaxies are 'centrals' in their respective haloes and are resolved with have more than 600 000 particles (dm+gas+stars) within the virial radius.[2] Since our aim is to study the impact of galaxy formation on the DM distribution, it is very important to use realistic simulated galaxies, i.e. galaxies able to reproduce the observed scaling relations. One of the key success of the NIHAO galaxies is to be able to reproduce the observed stellar mass–halo mass relation across the whole mass spectrum, which extends for more than five orders of magnitude in stellar mass, as shown in Fig. 1. As detailed in Wang et al. (2015), the NIHAO galaxies are also able to reproduce the stellar mass–halo mass relation also at higher redshift, and have realistic star formation rates for their stellar masses. NIHAO galaxies are also consistent with the observed gas content of galaxy discs and haloes (Stinson et al. 2015; Wang et al. 2016; Gutcke et al. 2016). Thanks to the unprecedented combination of high-resolution and large statistical sample, the NIHAO suite offers a unique tool to study the distribution response of several DM properties to galaxy formation.

Since among our goals there is the study of the shape of the DM distribution at different radii, it is interesting to check how these radii compare to the size of the central stellar region. Fig. 2 shows a histogram of the ratio between the stellar half-mass radius,

[2] In this paper, we have used the latest compilation of NIHAO galaxies, including several new 'central' galaxies that were completed after the publication of the first NIHAO paper.

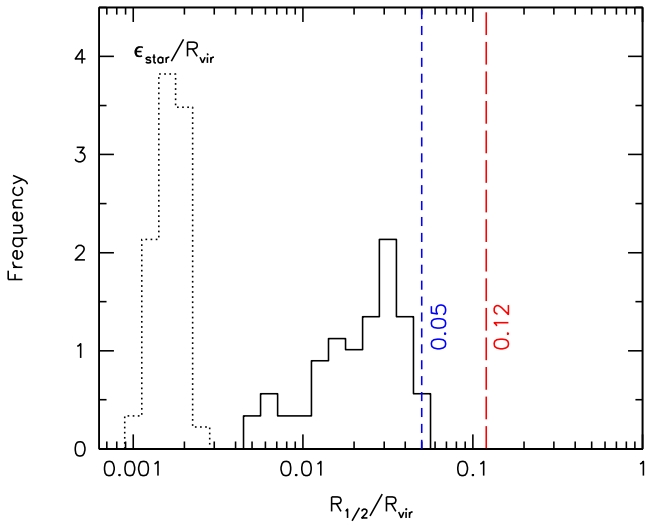

Figure 2. Histogram of the ratio between stellar half-mass radius, $R_{1/2}$, and the viral radius, $R_{\rm vir}$. For reference, the three radii at which we will compute the halo shape are: $R_{\rm vir}$, 12 per cent $R_{\rm vir}$ (red line) and 5 per cent $R_{\rm vir}$ (blue line). The leftmost histogram shows the distribution of the stellar particle softening through NIHAO.

$R_{1/2}$, and the viral radius, $R_{\rm vir}$. The three key radii at which we will compute the halo shape are: $R_{\rm vir}$, 12 per cent $R_{\rm vir}$ and 5 per cent $R_{\rm vir}$. As the plot shows, all these radii are larger than the size of the stellar body and are well above the softening of the simulations which is shown by the leftmost histogram in the figure (see also Table 1 and Wang et al. 2015). Finally, we have decided to use as minimum radius for our profiles 2 per cent of $R_{\rm vir}$, which again is well within the softening of all simulations. A more detailed discussion of the 'convergence radius' of our simulations can be found in Tollet et al. (2016).

In order to organize our results, we have decided to show detailed results (as, for example, the triaxiality parameter as a function of radius) for only four 'test' galaxies. These galaxies have masses equally spaced by half a dex ranging from 5×10^{10} to 10^{12} and are listed in Table 1. A visual impression of our galaxies is shown in Fig. 3, and was created using the Monte Carlo radiative transfer code SUNRISE (Jonsson 2006). The image brightness and contrast are scaled using arcsinh as described in Lupton et al. (2004). Around the mass, each of those galaxies we have then constructed a (total) mass bin of size of 0.5 dex (i.e. the mass bin around g1.08e11 goes from 7.5×10^{10} to 2.5×10^{11} $M_\odot$). No other selection criterion is used besides the mass. In the following, for all inspected DM properties (shape, phase-space and velocity distribution), we will present results for our single test galaxies and then average results for the four mass bins: M0–M3, listed in increasing mass order.

3 RESULTS

To determine the properties of the DM halo, we considered all DM particles within $R_{\rm vir}$ (the radius that encompasses a density equal to 200 times the critical density of the Universe) found using the Amiga Halo Finder (Knollmann & Knebe 2011). The study makes a direct comparison between the haloes that form in the DM-only simulations (black symbols in each figure) and those that form in the hydro simulations (red symbols).

The comparison is made between the axis ratios (b/a, c/a and T the triaxiality), the pseudo phase space density (Q), and the velocity distribution. We investigate the velocity dispersion both globally and in the Solar neighbourhood.

3.1 Halo shape

For each simulation (DM-only and hydro), we define the principal axes of the shape ellipsoid, such that $a > b > c$ and define the ratio parameters as $s = c/a$, $q = b/a$, $p = c/b$. To calculate the shape of the DM within a given radius, we begin with the assumption of a spherical ellipsoid, such that $a = b = c$. We then compute the inertia tensor I_{ij}, defined as

$$I_{ij} = \Sigma_\alpha m_\alpha x_i^\alpha x_j^\alpha / r_\alpha^2,$$

where m is the particle mass, α is the particle index and i, j refer to the coordinates. The radius is defined to be $r_\alpha^2 = x_\alpha^2 + y_\alpha^2/q^2 + z_\alpha^2/s^2$ (Kazantzidis et al. 2004).

The eigenvalues of this matrix produce new values for s, q, p. We iterate, using the eigenvalues of the previous matrix as the new assumptions of s and q, until the fractional difference of s, q, p converges to a tolerance value of 10^{-3} (Macciò et al. 2008).

Finally, we define the triaxiality parameter as $T = [1 - (b/a)^2]/[1 - (c/a)^2]$. A prolate halo has $T = 1$, and oblate halo has $T = 0$, while a triaxial halo has $T \sim 0.5$.

In Fig. 4, we present the relation between the minor to major axis ratio (c/a, left) the middle to major (b/a, centre) and the triaxiality parameter (right) as a function of radius. The solid line is for the integral measurement of the shape (i.e. $c/a(< r)$), while the dotted line is for the differential one. In each panel, the last point marks the virial radius of the halo. As discussed previously, for clarity and brevity, we present results only for our 4 test galaxies (see Table 1) out of 93 in our sample,

The trend is similar across all masses: baryonic physics processes, such as cooling and stellar feedback, modify the shape of the DM distribution. The effect of baryons physics is strongest at the centre of the halo. In general, the hydro simulations have a less varying shape as a function of radius with respect to N-boby sims and the hydro shape is always rounder than the DM. At small radii, the DM becomes more triaxial. Near $R_{\rm vir}$, the shapes of the hydro and DM-only simulations converge to their most spherical shape in all the galaxies except the most massive one, g1.92e12.

Table 1. Properties of the four selected 'test' galaxies. M_* is the total stellar mass within $R_{\rm vir}$. Note that in the NIHAO project, the 'name' of a galaxy indicates the mass of the halo in the DM-only simulation.

Simulation name	M_* ($M_\odot$)	$R_{\rm vir}$ (kpc)	Softening (pc)	$m_{\rm DM}$ ($M_\odot$)	$m_{\rm gas}$ ($M_\odot$)	$N_{\rm vir}^{\rm DM}$	$N_{\rm vir}^{*}$	Mass bin name	Mass range ($M_\odot$)
g1.92e12	1.59e+11	281	931	1.74e+06	3.16e+05	1200 667	2467 821	M3	7.5e+11<$M_{\rm vir}$ <3.5e+12
g5.02e11	1.46e+10	179	465	2.17e+05	3.95e+04	2408 247	1821 403	M2	2.5e+11<$M_{\rm vir}$ <7.5e+11
g1.08e11	8.47e+08	105	465	2.17e+05	3.95e+04	520 108	108 025	M1	7.5e+10<$M_{\rm vir}$ <2.5e+11
g4.99e10	1.24e+08	78	207	1.90e+04	3.48e+03	732 808	52 511	M0	4.0e+09<$M_{\rm vir}$ <7.5e+10

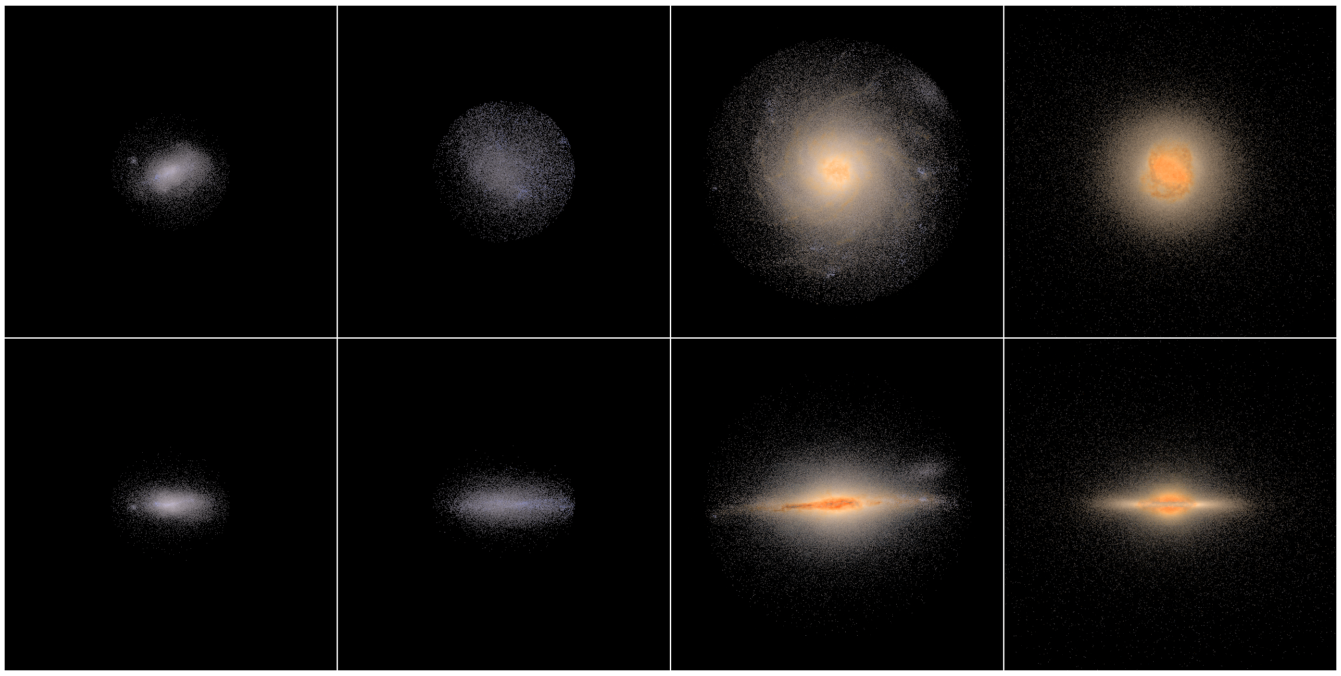

Figure 3. Face-on (upper panels) and edge-on (lower panels) views of our four selected 'test' galaxies: g4.99e10, g1.08e11, g5.02e11, g1.92e12 from left to right. Galaxies have been processed through the Monte Carlo radiative transfer code SUNRISE. Images are 50 kpc on a side.

Fig. 5 shows the same quantities as in Fig. 4 but this time averaged over the four mass bins M0–M3 (see Table 1), with the grey area representing the 1σ scatter around the mean. The radius at which DM-only and hydro results depart from each other moves to larger radii as the mass grows. In the lowest mass bin (M0, lowest row), there an appreciable difference between DM-only and hydro-only inside few kpc, while in the most massive bin (M3, uppermost row) the difference is already substantial at 100 kpc. This is true for all three diagnostics. Overall, the general trends are quite in agreement with the ones from our test galaxies, which appear to provide a good representation of the general population; on the other hand, this figure also points out the not-so-negligible galaxy-to-galaxy variations in the response of haloes to baryons.

Debattista et al. (2008) described how the condensation of baryons into galaxy centres affect the DM shape. DM-only simulations produce haloes with a prolate shape, $\frac{1}{2}a \sim b \sim c$. Maintaining the prolate shape relies on DM staying on box orbits. A prime characteristics of box orbits is that they make close passages past the halo centre. As baryons cool and collapse into the centre, they deepen the potential well there and scatter material from box orbits into rounder loop or tube orbits. Tube orbits have an oblate shape, $a \sim b > c$. Figs 4 and 5 show the gradual transition of inner halo shapes from prolate towards oblate as the mass increases: b/a increases to 1 more quickly than c/a.

In order to better quantify the difference in shape between DM-only and NIHAO simulations on a galaxy-by-galaxy base, we have decided to compare results for all three shape diagnostics (b/a, c/a and T) at three specific radii: $R_{\rm vir}$, 12 per cent $R_{\rm vir}$ and 5 per cent $R_{\rm vir}$.[3]

[3] The difference in $R_{\rm vir}$ between DM-only and hydro is always of the order of few per cent and hence does bias our results.

The virial radius has been chosen to have the possibility to make a direct comparison with previous studies based on DM-only simulations (Jing & Suto 2002; Allgood et al. 2006; Bett et al. 2007; Macciò et al. 2008). On the other hand, observationally measuring the shape of DM haloes at the virial radius is a quite difficult task since there are very few (if any) tracers of the DM shape (or potential) that extend so far from the galaxy centre. We have then decided to look at the halo shape at $0.12 \times R_{\rm vir}$, which is in the middle of the 20–60 kpc radius range of the halo that Ibata et al. (2001) state shaped the Sagittarius stream. Finally, we also look at the shape in the very inner part of the halo (5 per cent $R_{\rm vir}$), which is the most prone to be affected by baryonic effects.

Fig. 6 shows the value of the three shape diagnostics as a function of the total mass of the halo, at our three reference radii. At the virial radius, at all masses, the NIHAO galaxies and their DM-only counterparts show very similar values for the axis ratio and triaxiality, and in agreement with results obtained from larger samples of simulated DM haloes (Macciò et al. 2008, black solid line in the first and second panel).

At smaller radii (second and third rows), there is a steady increase of c/a (and b/a) with $M_{\rm vir}$ in the NIHAO simulations, which brings the simulated values in good agreement with the MW observations of Ibata et al. (2001, green circle). The last column in Fig. 6 shows the triaxiality parameter versus halo mass, confirming that CDM haloes are typically prolate (black squares). Interestingly, when galaxy formation is included, the full range of halo triaxialities is possible (red diamonds).

The difference between hydro and DM-only simulations can be better appreciated in Fig. 7, where we show the ratio between the halo shapes c/a (left), b/a (centre) and T (right) between collisional and collisionless simulations as a function of halo mass. The figure shows that there is a consistent shift for the inner halo shape from the DM-only to the baryon simulation and the trend of halo shapes becomes more spherical with increasing halo mass is clearly visible.

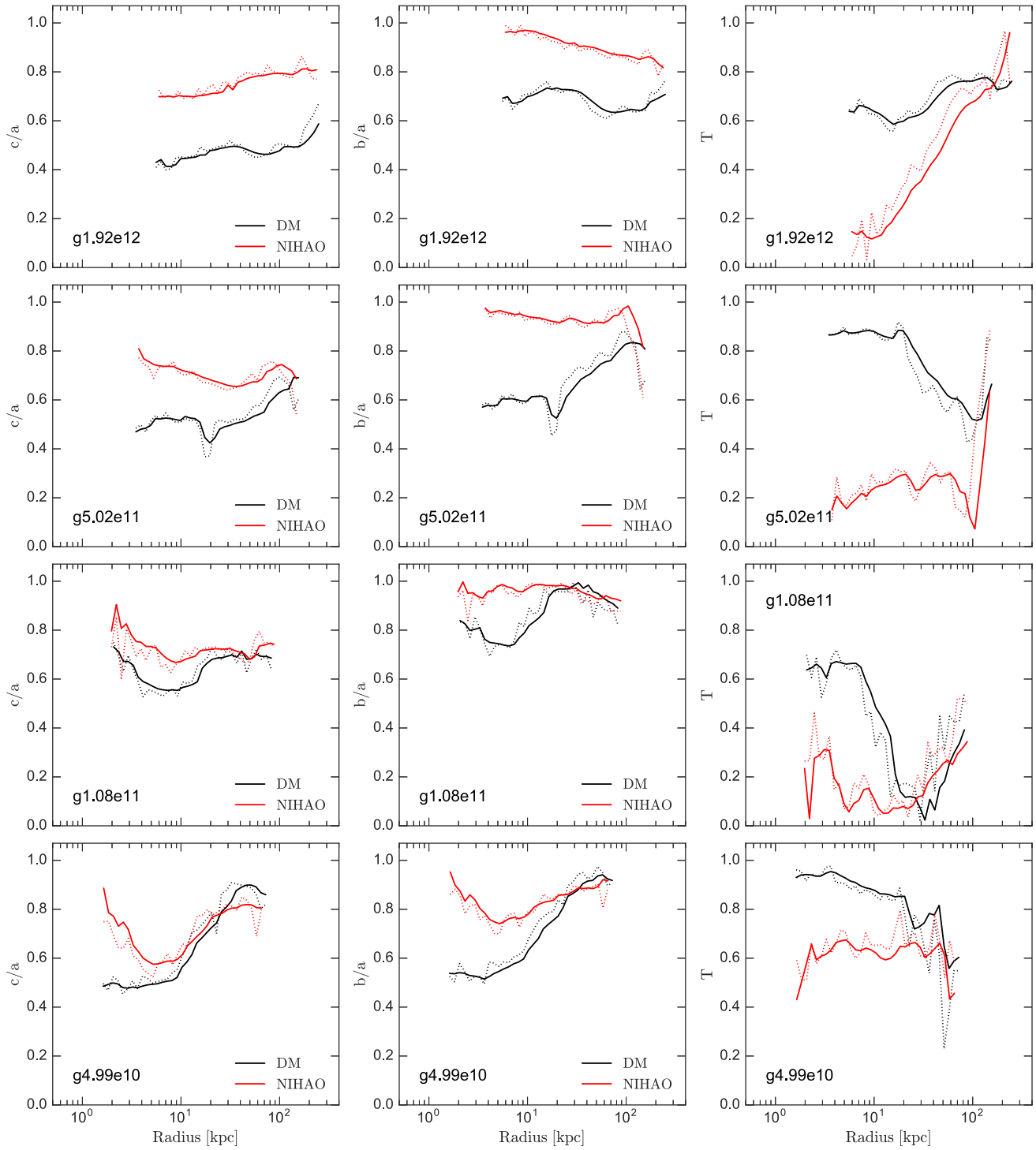

Figure 4. Ratio of minor-to-major axes (c/a, left), middle-to-major axes (b/a, centre) and triaxiality (T, right) as a function of radius. DM-only simulations are depicted in black, while hydro (NIHAO) simulations are depicted in red. Both the integral (solid line) and differential (dotted line) values are shown.

For the left-middle panel (0.12 $R_{\rm vir}$, the most accessible to observations), we decided to fit such a ratio with a simple S-shape function:

$$S(M) = s_1 + \frac{(s_2 - s_1)}{1 + (M/\mathrm{M}_0)^{\beta}}, \quad (1)$$

where M is the virial mass of the halo. We fixed the value of the s_2 parameter to 1.0 and fit for the other ones using the Levenberg–Marquardt method, results are reported in Table 2. The final fitting function is shown by the black line in Fig. 7, while the grey area represents the $1\sigma = 0.156$ scatter around the mean.

The trend of shape change with halo mass can be understood as a consequence of the increased efficiency of star formation of

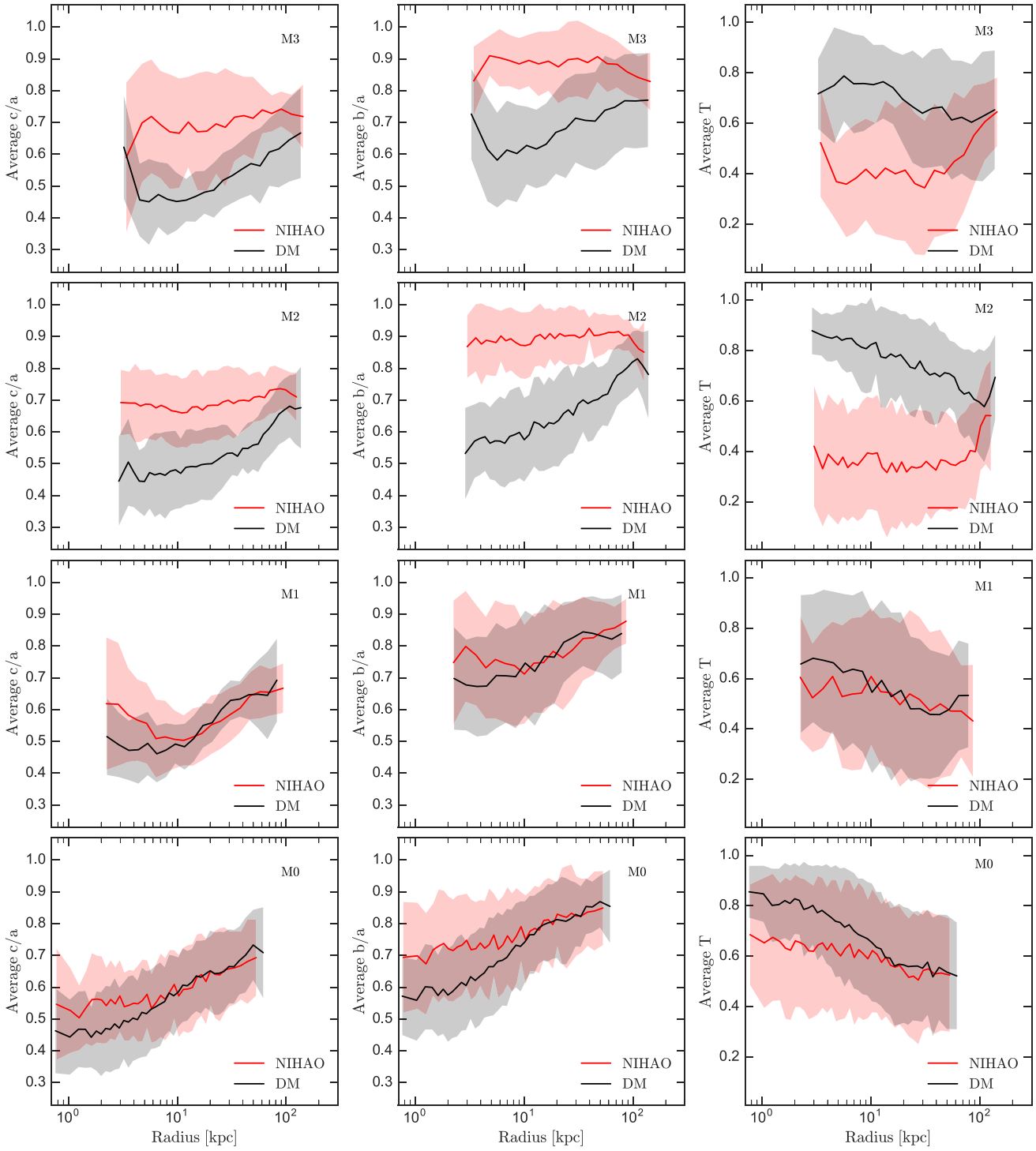

Figure 5. Same as Fig. 4 for all galaxies in the four mass bins M3–M0 (M0 < M1 < M2 < M3 $\sim 10^{12}$ $M_\odot$). The shaded area represents the 1σ scatter from galaxy to galaxy in the respective mass bin. Only the integral shape (solid line) is shown.

massive haloes (in our sample, e.g. 10^{12} $M_\odot$) with respect to low-mass ones, as implied by abundance matching (Moster et al. 2010). Fig. 8 shows the different shape measurements versus the ratio between the stellar and the total mass. Since there are no stars in the DM-only simulation, we use the empirical formula of Moster et al. (2010) to assign a stellar mass to each halo (black squares).

As expected for a very low values of $M_*/M_{\rm vir} < 0.01$, the influence of baryons is minimal and the halo shape does not change substantially between DM-only and hydro simulations. For larger values of the stellar-to-total mass ratio, the two distributions tend to diverge, with the NIHAO galaxies showing a substantially rounder halo shape.

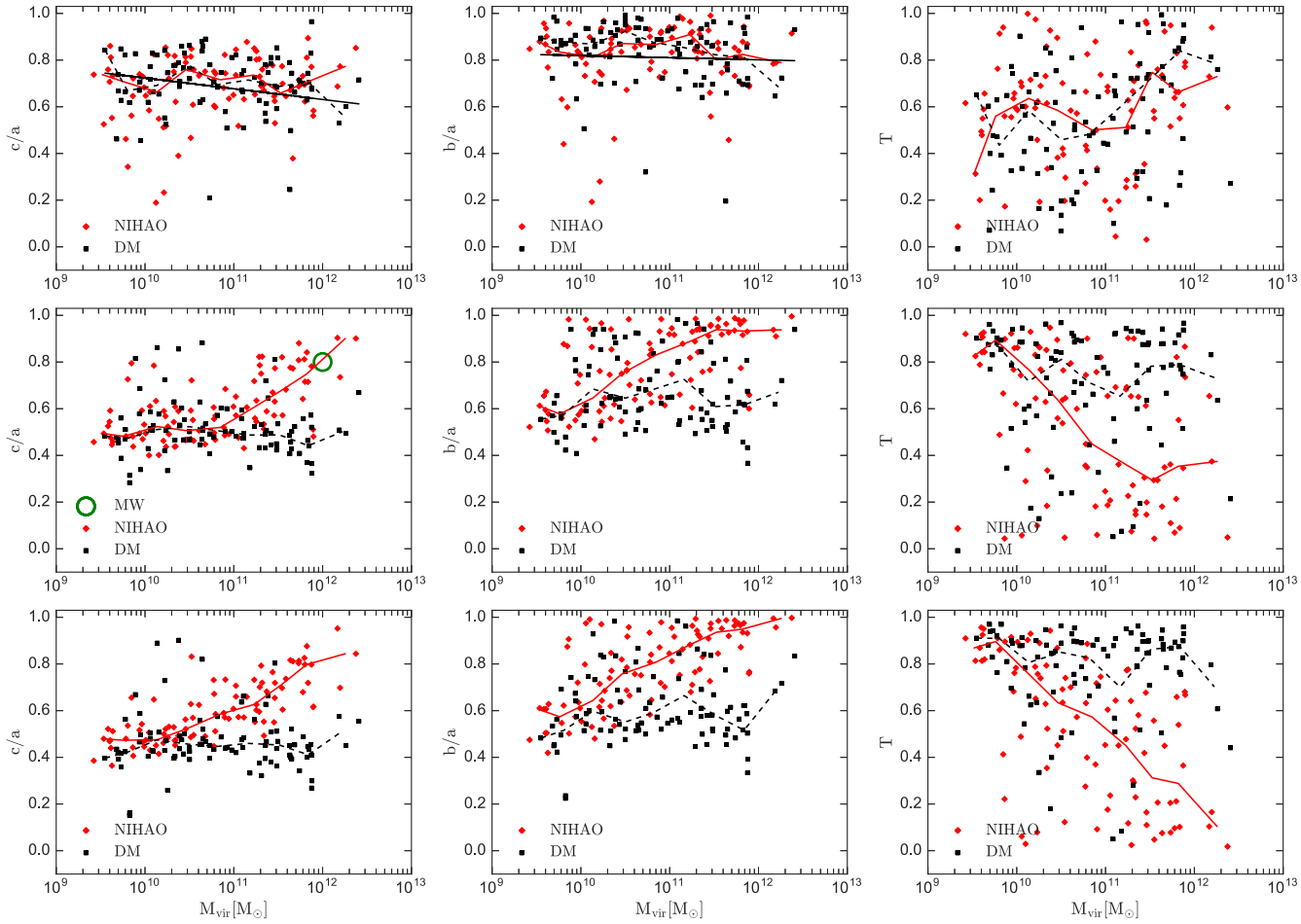

Figure 6. Axis ratios (c/a, b/a) and triaxiality parameter (T) for all the galaxies as a function of their virial (total) mass. The first row shows results at the virial radius, the middle row results at 0.12 of R_{vir} and the last row at 5 per cent of R_{vir}. Red diamonds represent the NIHAO galaxies, while black squares show the corresponding results for the DM-only runs. The solid lines in the first and second panel show the relation from Macciò et al. (2008). The green circle in the middle-left panel shows the halo shape measurement for the Milky Way from Ibata et al. (2001). The red (black) line shows the median value for the hydro (DM) results.

A similar trend also applies to the triaxiality parameter (last columns). When galaxy formation is very inefficient ($M_{star}/M_{vir} < 0.01$), haloes retain their prolate shape. Above ($M_{star}/M_{vir} > 0.01$), haloes can become both triaxial $T \sim 0.6$ and close to oblate $T \sim 0.2$. This is quite important since, when embedded within a triaxial DM halo, there can be systematic differences between the rotation speed and the circular velocity in gaseous discs, which has important implications for interpreting observations of DM density profiles (Hayashi & Navarro 2006).

The shape of the halo leaves an imprint on the 2D kinematics (Kuzio de Naray & Kaufmann 2011), with triaxial haloes yielding twists along the minor axis, and spherical (or aligned axisymmetric) haloes yielding symmetric velocity fields. Our simulations thus predict a wider diversity of kinematic structures than would be inferred from DM-only simulations.

Recently, Kazantzidis, Abadi & Navarro (2010) have used controlled (N-body) experiments to study the effect of the growth of a disc on to a triaxial halo. They found that the net effect depends weakly on the time-scale of the disc assembly but strongly on the overall gravitational importance of the disc.

In order to test their results on the importance of the baryonic mass (stellar and gaseous)[4] contribution to the local potential in Fig. 9, we show the baryonic fraction, $[M_{gas}(R) + M_*(R)]/M_{tot}(R)$, computed at $R = 5$ per cent, R_{vir} (green) and 12 per cent, R_{vir} (blue), as a function of halo mass. Let us underline that our galaxies are very realistic stellar masses (see Fig. 1) and hence our baryonic fractions should be minimally effected by a possible overcooling. A comparison of this figure with Fig. 7 shows that a difference between DM-only and hydrodynamical simulations becomes clear only when the baryonic (mostly stellar) mass is at least of the order of 10 per cent of the total one, supporting the findings of Kazantzidis et al. (2010).

Finally, before concluding our section on the DM halo shape, we want to look at the effects of the shape of the stellar component (i.e. the galaxy morphology) on the final halo shape. Fig. 10 shows the relation between the shape of the stellar component (computed at 5 per cent R_{vir}, radius that includes more than 90 per cent of all

[4] Since we have fully cosmological simulations, we have decided to use the global baryonic contribution and not just the disc one.

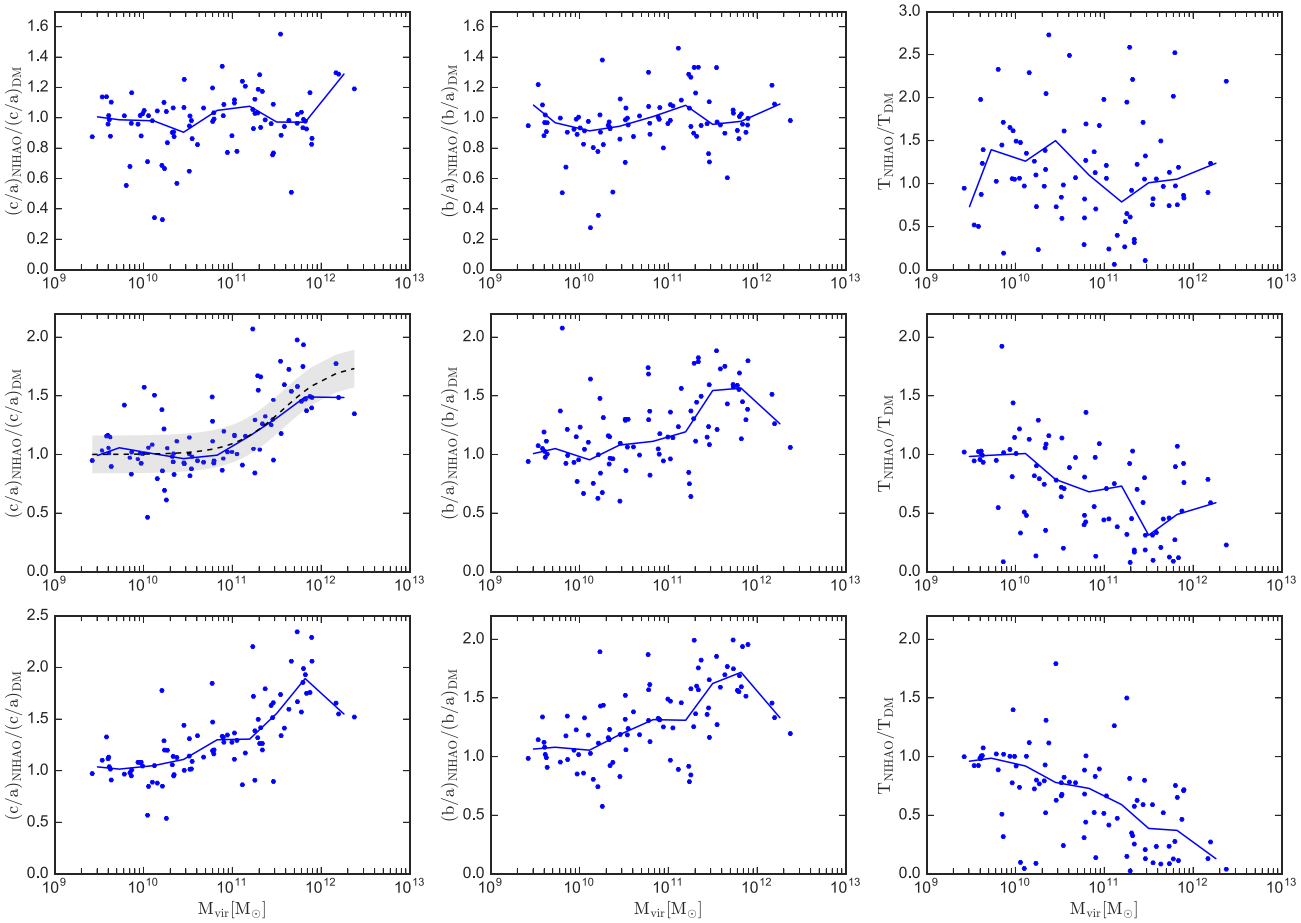

Figure 7. Ratio between the halo shape (c/a) in the NIHAO and DM-only simulations as a function of the halo mass. The first row shows results at the virial radius, the middle row results at 0.12 of R_{vir} and the last row at 5 per cent of R_{vir}. The dashed line in the middle-left panel is the fitting function provided in equation (1), the grey area is the 1σ scatter around the mean. The blue line shows the median value.

Table 2. Fitting parameters describing the ratio between the halo shape, c/a, at 0.12 R_{vir} in the hydro and DM-only simulations (middle-left panel of Fig. 7).

s_1	s_2	M_0 ($M_\odot$)	β
1.848	1.0	3.1×10^{11}	1.49

stars) and the relative change in the inner shape (12 per cent, R_{vir} upper panel and 5 per cent, R_{vir} lower panel) between NIHAO and the DM-only run. In order to avoid to mix the effect of halo mass with the effect of stellar morphology, this plot has been done using only galaxies in the M2 mass bin.

On the larger spatial scale, the correlation (if present) is very weak, while a positive trend is more apparent on the very small scale of 5 per cent R_{vir}. On this scale, it looks that a more spherical stellar distribution causes stronger change in the DM halo shape. This correlation can be explained by the fact that rounder stellar bodies (i.e. bulges) are more compact than disc ones and hence more effective in modifying the orbit of DM particles (e.g. Debattista et al. 2008).

3.2 DM pseudo phase-space density

Moving beyond the morphology of the DM, it is possible to also consider its kinematics. Taylor & Navarro (2001) defined 'pseudo phase-space density' as a simple relationship between matter density and velocity dispersion, a quantity that describes the matter distribution and kinematics of the DM together. They defined pseudo phase-space density as

$$Q(r) = \rho(r)/\sigma^3(r),$$

where $\sigma(r)$, $\rho(r)$ are the velocity dispersion and density of the halo, respectively. Taylor & Navarro (2001) found that this simple combination of properties serves as a useful probe for understanding the origin of the universal DM halo profiles.

Using DM-only simulations, Taylor & Navarro (2001) found that the pseudo phase-space density follows a simple power law, $Q(r) \propto r^\chi$, with $\chi \sim -1.875$. Since there is mounting evidence that baryons modify the DM density profile, $\rho(r)$, (e.g. Mashchenko, Couchman & Wadsley 2006; Governato et al. 2010; Teyssier, Johnston & Kuhlen 2012; Di Cintio et al. 2014a; Tollet et al. 2016), it is worth checking whether baryons also reshape the Q profile.

Fig. 11 presents a comparison between the matter density profile (right) and the pseudo phase-space density Q profile (left) for our 'test' galaxies (the same galaxies shown in Fig. 4). Each density profile includes three lines: the density in the DM-only simulations (black solid line), the DM density in the hydro simulations (red solid line) and the total density profile (dark+stars+gas) in the hydro simulations (red dotted line). While profiles from DM-only simulations have universal Einasto-like shapes (e.g. Navarro et al.

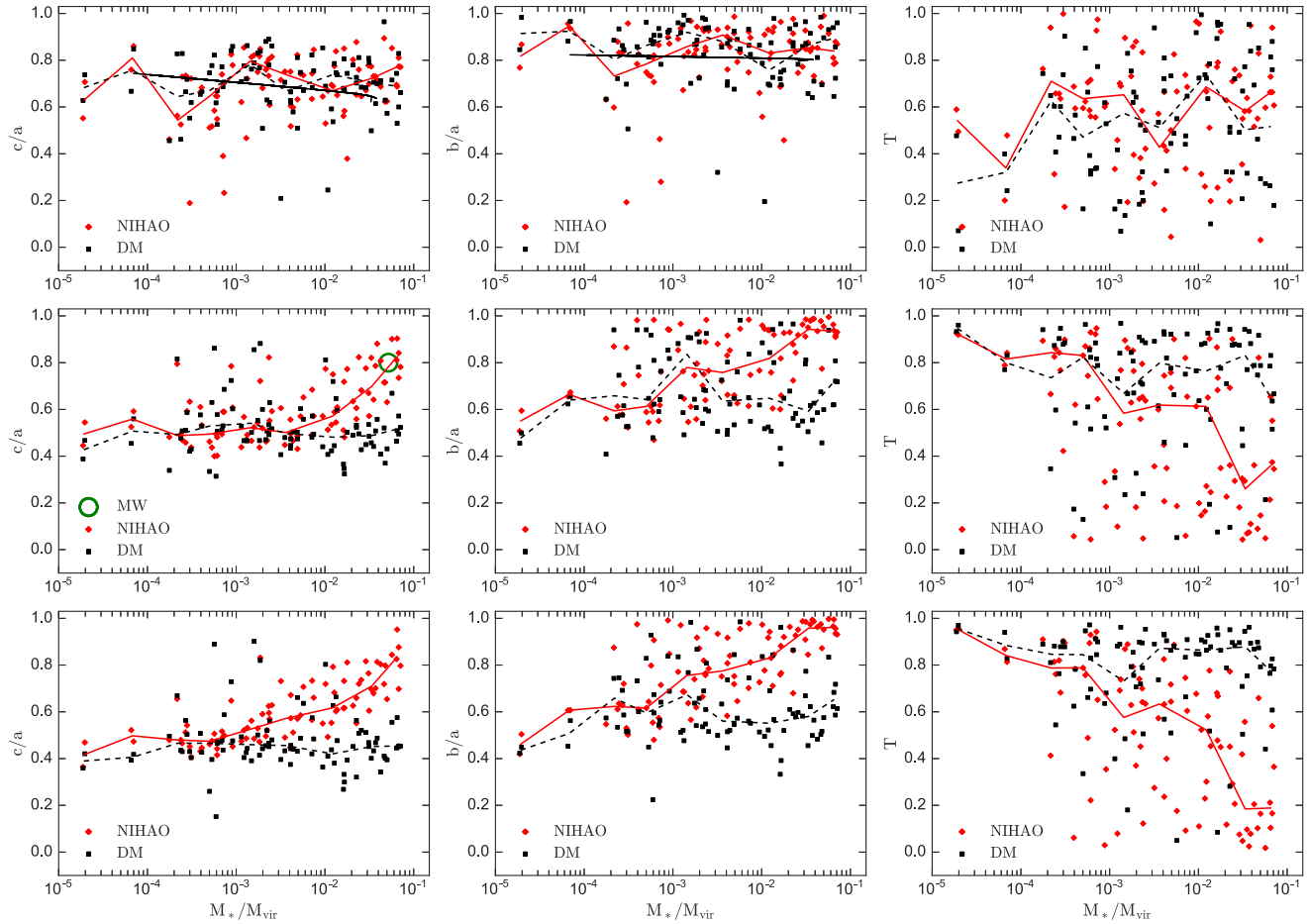

Figure 8. Same as Fig. 6 but this time as a function of the star formation efficiency of the halo, parametrized as M_*/M_{vir}. The values for M_*/M_{vir} for the DM-only simulation are obtained using the relation from Moster et al. (2010). The red (black) line shows the median value for the hydro (DM) results.

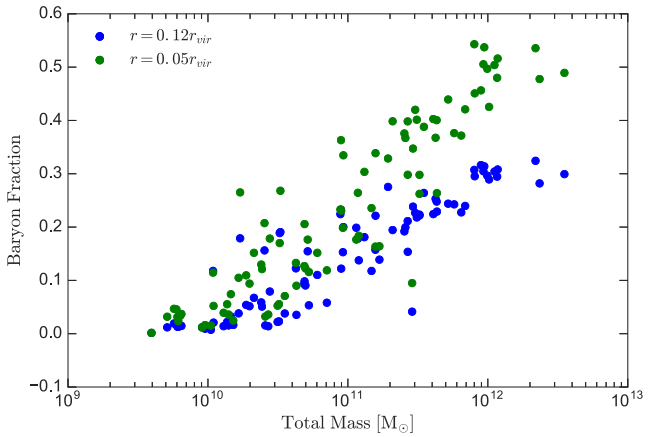

Figure 9. Baryon fraction at 12 per cent (green) and 5 per cent (blue) of R_{vir} as a function of total mass. It is clear that baryons start to be significant only above a total mass of few 10^{11} M$_\odot$.

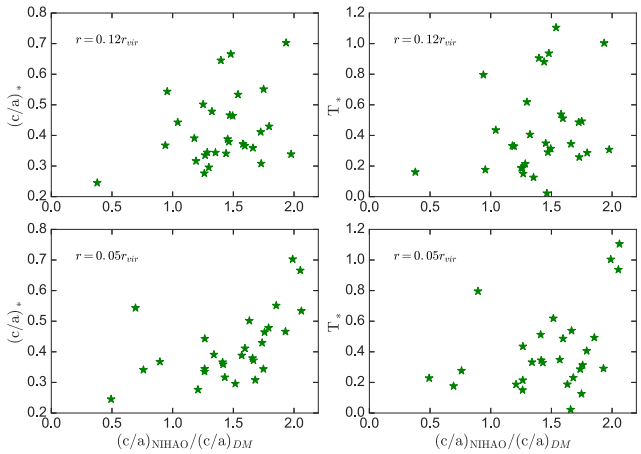

Figure 10. Relation between the shape of the stellar component and the relative change in the inner shape (12 per cent R_{vir} upper panel and 5 per cent R_{vir} lower panel) between NIHAO and the DM-only run.

2004; Merritt et al. 2005; Dutton & Macciò 2014), profiles from hydro simulations exhibit a core for low-mass haloes which gradually steepens with halo mass, becoming even more cuspy DM-only simulations of the most massive galaxies in our sample (see Tollet et al. 2016 for a thorough discussion of the modification of the DM density profiles in the NIHAO simulations).

The Q profiles show a different behaviour. Q in hydro simulations is always lower than its N-body counterpart. The profiles also flatten in the centre even when the density profiles do not. The flattening of Q in the lowest mass halo (bottom panel) reflects the flattening of the matter density, which decreases the numerator in the definition

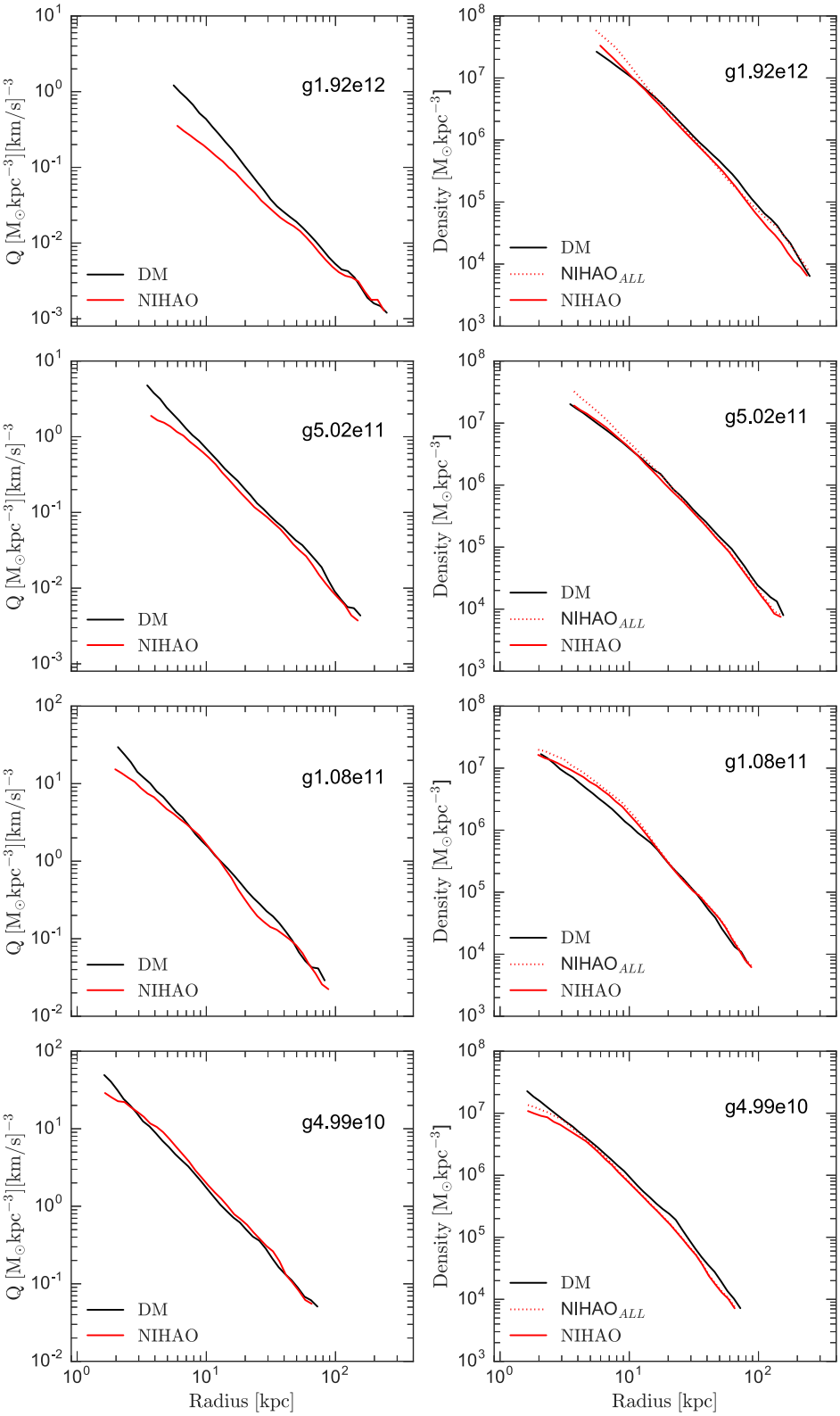

Figure 11. The density (left) and pseudo phase-space density (right) of DM-only (black) and NIHAO (red) galaxies for our four test objects. Solid lines represent the density and Q values of the dark matter particles, while the red dotted line represents the total density of the star, gas, and dark matter particles.

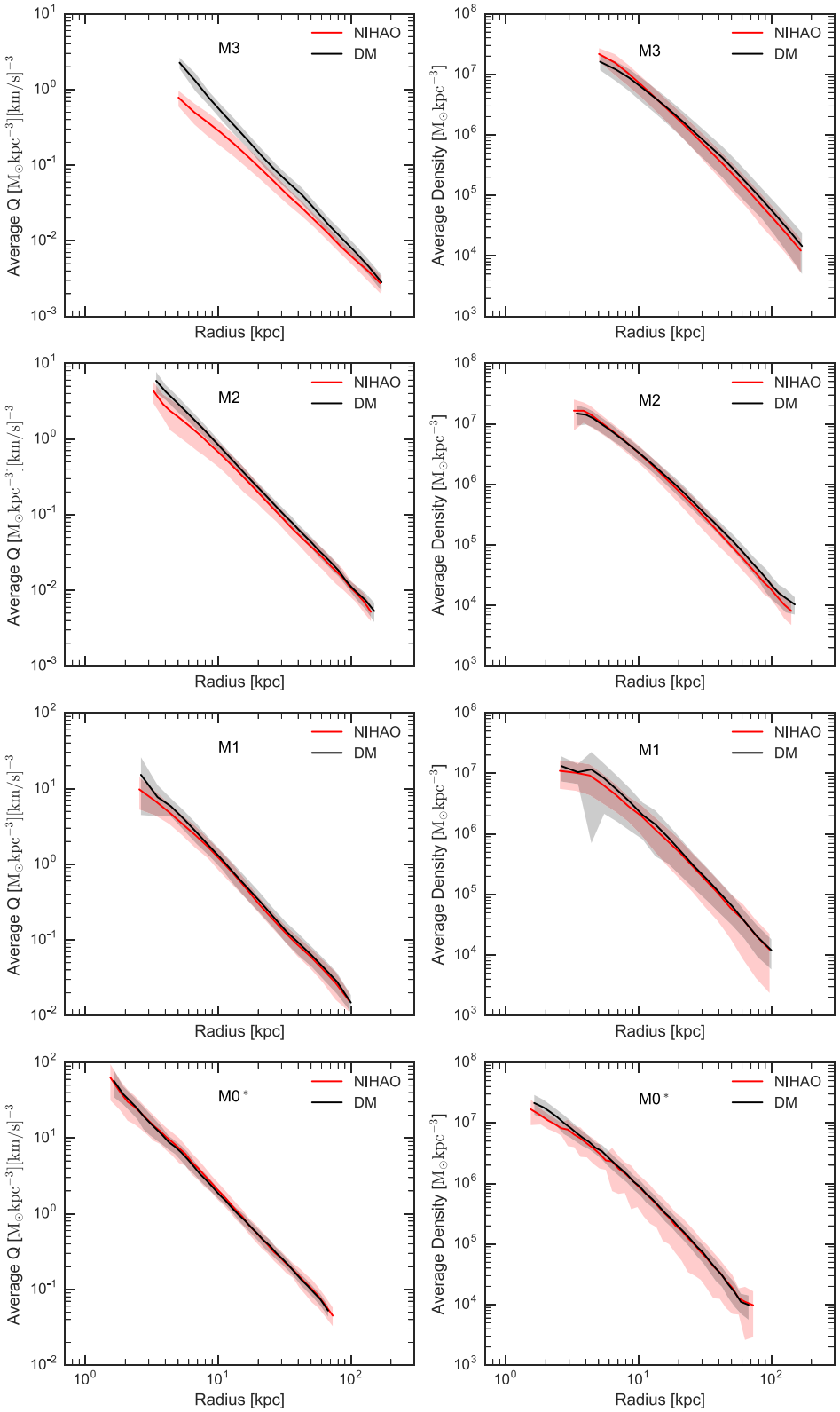

Figure 12. The density (left) and pseudo phase space density (right) of DM-only (black) and NIHAO (red) galaxies averaged in the for mass bins M0–M3 (M0 < M1 < M2 < M3 $\sim 10^{12}$ $M_{\odot}$). The grey area represents the 1σ scatter around the mean.

of Q. For the other three panels, there is no such discrepancy in the matter density profile. However, the 'total' density profile in the hydro simulation does get steeper in all three cases. The deeper global potential well causes the velocity dispersion of the DM σ to increase towards the centre, thus flattening the inner part of the Q radial profile. As a consequence, the pseudo phase-space density profile of the DM component departs from simple power-law behaviour at practically all mass scales probed by our hydrodynamical simulations.

A comparison of Figs 4 and 11 also suggests that the violent gas motions caused by baryons in the centre of low-mass galaxies which are believed to be responsible of the flattening of the central DM cusps (e.g. Pontzen & Governato (2012)), also works to make the DM rounder. In the low-mass g4.99e10, baryons make little change to the outer shape of the DM. However, the DM is almost completely spherical inside 2 kpc, the same region in which the density profile has been flattened.

Fig. 12 shows the same quantities as in Fig. 11 but this time averaged for all galaxies in the different mass bins M0–M3. The averaged profiles confirm the trends already seen for the four 'test' galaxies. In the lowest mass bin (M0), there is quite small difference between the averaged Q computed in the DM-only or NIHAO simulations, suggesting that stochasticity of star formation is quite strong on those mass scales as already pointed out in works dealing with the flattening of the density profiles (e.g. Oñorbe et al. 2015; Tollet et al. 2016)

In Fig. 13, we try to summarize our findings by showing the ratio of the values of Q at two different radii in NIHAO and in DM-only simulations: 0.05 $R_{\rm vir}$ and 0.12 $R_{\rm vir}$. At low masses (M$\approx 10^{10}$ M$_\odot$), there is no much difference between the two Qs; at higher masses, the hydro simulations show, on average, a lower value of Q, in agreement with findings based on single profiles. Most likely, this strong dependence of the Q ratio on halo mass is due to the σ^3 term in the denominator of the definition of the pseudo phase-space density. The density when computed at 5 per cent or $R_{\rm vir}$ (lower panel of Fig. 13) shows an average lower value in the hydro simulations up to a mass of few 10^{11} solar masses, and similar values above this mass, consistent with results on halo expansion and contraction reported in Tollet et al. (2016).

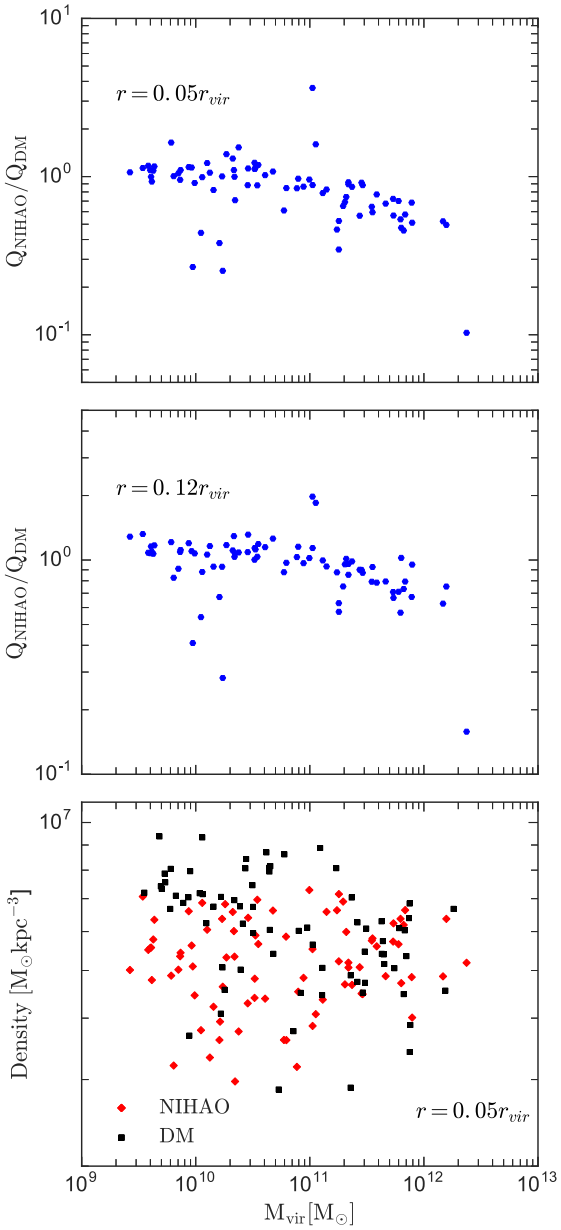

Figure 13. The top panel shows the ratio of the values of Q in the in dissipationless and hydro simulations computed at 0.05 $R_{\rm vir}$(0.12 $R_{\rm vir}$ for the middle panel). The outliers in the plot are due to merging galaxies (haloes) which are at a slightly different merging state in the hydro and DM simulations. The bottom panel shows the values of ρ at 5 per cent of $R_{\rm vir}$ for the DM (black) and the NIHAO (red) simulations.

3.3 DM velocity distribution

As outlined in the introduction, the velocity distribution is crucial for the detection of DM in the Milky Way. For this reason, together with the results of our test galaxies, and the corresponding averaged mass bins (M0–M3), we will also show results for four more single galaxies namely: g8.26e11, g1.12e12, g1.77e12, g2.79e12.

These galaxies have been selected in order to have a stellar and halo mass similar to the one of our own Galaxy ($\approx 10^{12}$ M$_\odot$), three of them (g8.26e11, 1.77e12 and g2.79e12) are strongly disc dominated with a disc to total ration of $D/T > 0.6$ (computed according to Obreja et al. 2016), while g1.12e12 is quite compact with the disc accounting for $\sim$10 per cent of the total stellar mass. Edge-on and face-on images of these four galaxies are shown in Fig. 15. Each image is 50 kpc on a side and was created using the Monte Carlo radiative transfer code SUNRISE (Jonsson 2006).

Fig. 14 shows the velocity distribution of DM on two different scales for our test galaxies. The first row of Fig. 14 shows the distribution of all DM particles within the virial radius, while the second row shows the distribution only inside the solar neighbourhood. This quantity is defined as a shell of radius within the range 7 kpc $< r <$ 9 kpc for galaxies in the M3 mass bin, and it is then rescaled to a similar fraction of the virial radius (around 4 per cent) for lower mass galaxies. In principle, the solar neighbourhood should be defined as a ring in the plane of the disc with radius between 7 and 9 kpc. We tested on our more disc-dominated galaxies (g8.26e11, g1.77e12, g1.92e12, g2.79e12) that the results do not change at all if we use a spherical shell instead, which has two advantages: it

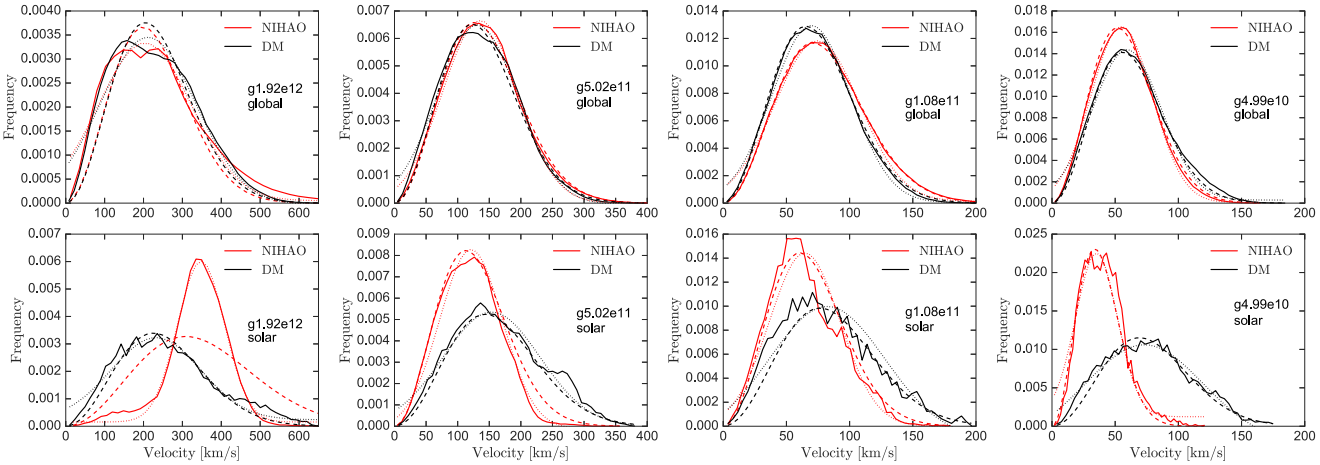

Figure 14. The dark matter particles velocity distribution in our four test galaxies. The dashed lines indicate a Maxwellian fit to the simulated curves. The top panels show the global velocity distribution, while the bottom panels show local measurements taken at the solar position($7\ \mathrm{kpc} < r < 9\ \mathrm{kpc}$) for galaxies in the M3 mass bin, and a similar fraction (≈5 per cent) of the virial radius for lower mass galaxies. For the local velocity distribution, the dotted line shows a Gaussian fit to the NIHAO curve.

increases the number of DM particles (and thus reduces the numerical noise) and can be applied to both hydro and DM-only simulations. The similarity of results for a shell and a ring suggests that the DM distribution is spherically symmetric and no 'dark' disc is present in our simulations. The black lines in Fig. 14 show results from DM-only simulations, while red lines are for the NIHAO galaxies. At the virial radius, in both types of simulations, a Maxwellian distribution well represents the global velocity distribution:

$$f(x) = m_1 \frac{x^2 e^{-x^2/(2m_2^2)}}{m_2^3}. \quad (2)$$

The best-fitting Maxwell functions are shown as dashed lines in Fig. 14.

When restricted to the solar neighbourhood, the DM-only and the hydro velocity distributions differ substantially in all galaxies. The DM-only simulations can still be well fit with a Maxwellian distribution, (even if they show a slightly larger tail at high velocity). Kuhlen et al. (2010) found similar agreement using higher resolution simulations. In the hydro case, the velocity distribution for the most massive test galaxy (g1.92e12) is much more symmetric around the maximum value, which increases substantially, and then the distribution falls quite rapidly at high velocities. This difference is most likely due to the quite significant halo contraction for this galaxy (see Fig. 11) which boosts the local DM velocity dispersion.

This strong variation at the very high-mass end of the NIHAO galaxies is also confirmed by a closed inspection of the velocity distribution of the four additional high-mass galaxies shown in Fig. 16. With increasing mass, the distribution becomes more Gaussian and the peak moves towards larger velocities, but the fall-off at the high-velocity end is quicker than in the DM-only case. Despite the different aspect (see Fig. 15), the four galaxies have quite similar behaviour, suggesting that morphology is not the main driver of the changes in the velocity distribution, which seems to be more related to the total stellar (or halo) mass.

For smaller masses (g5.02e11, g1.08e11, g4.99e10), the peak of the distribution moves towards lower velocities, possibly related to the different halo response on these mass scales, where either expansion or no reaction (for $M_*/M_{\mathrm{halo}} < 10^{-4}$) is expected (Tollet et al. 2016).

As a consequence of baryonic effects, the local velocity distribution of MW-like galaxies is better fit by a Gaussian distribution:

$$f(x) = g_1 e^{-(x-\mu)^2/(2\sigma^2)}. \quad (3)$$

The Gaussian fit is shown in the lower panels of Figs 14 and 16 by the (red) dotted line that clearly provides a better fit than a Maxwellian (red) dashed line. The fitting parameters for both distributions (Gaussian and Maxwellian) are reported in Table 3, all fits have been performed using the Levenberg and Marquardt algorithm.

Finally, Fig. 17 shows the average velocity distribution and the virial radius (upper panels) and at the solar radius (lower panels). While the trend seen is individual galaxies confirmed in the M0–M2 bins (with g1.99e10 being a bit borderline), this figure also illustrates the non-negligible scatter in the galaxy-to-galaxy variation for the local velocity distribution.

In the highest mass bin (M3), the results previously highlighted get washed away due to the large scatter galaxy by galaxy, as marked by the extended red area. This scatter is due to the rapid change in halo response (from expansion to contraction) across this mass bin. For lower masses, the average values confirm trends seen previously on single galaxies, namely more symmetric distributions and a lower tail at high velocities.

On the Milky Way scale, our findings confirm earlier results based on the single halo ERIS simulation (Guedes et al. 2011) and presented by Pillepich et al. (2014). In their paper, Pillepich and collaborators also reported a suppression of the wings and a more symmetric shape for the velocity distribution. In our simulations, the differences between the DM-only case and the hydro simulations seem to be even larger. This discrepancy might be due to the stronger feedback model (which leads to a stronger baryonic impact) we have adopted in our simulations in order to balance the metallicity dependent gas cooling, which was ignored in the original ERIS simulation.

As extensively discussed in Pillepich et al., the suppression of the tail of the distribution at high velocities has important consequences on the interpretation and the comparison of different direct detection experiments. For example, it relaxes the tension between the (possible) signal of DM scattering reported by CDMS-Si (Agnese et al. 2013) and the exclusion of such a signal from the Xenon-100 experiment (Aprile et al. 2012). We refer the reader to Mao, Strigari

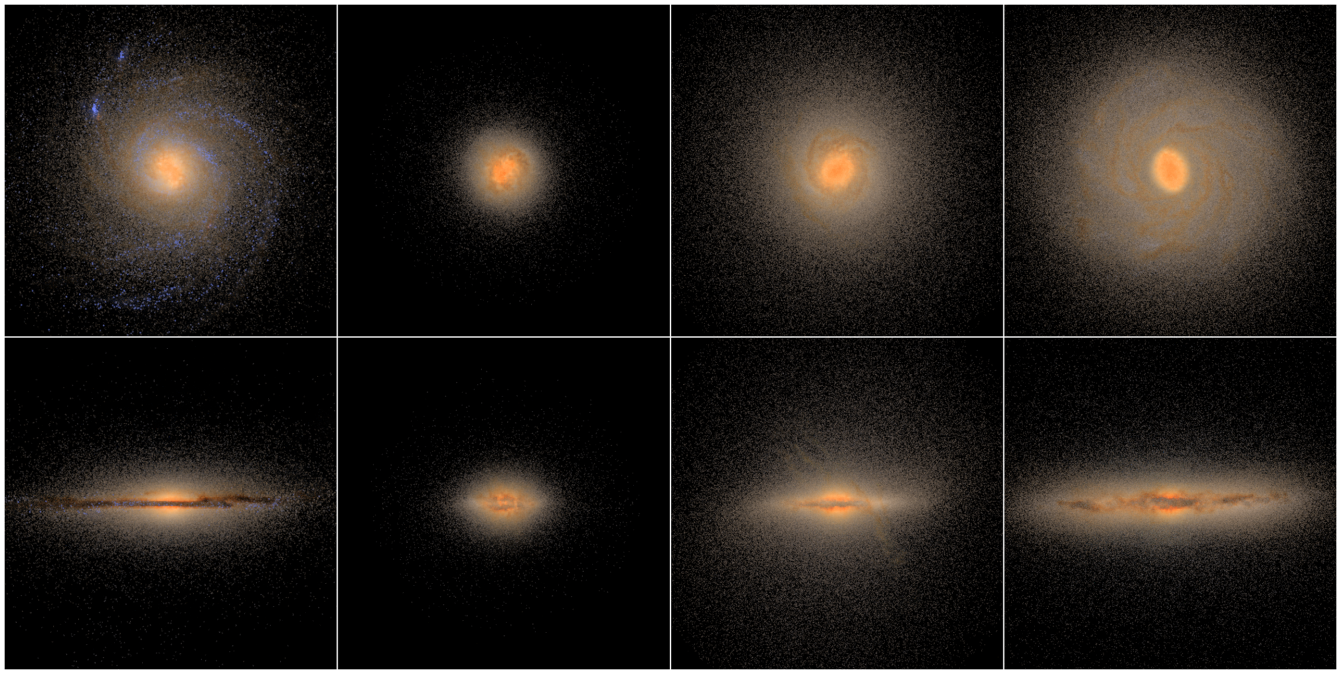

Figure 15. Face-on (upper panels) and edge-on (lower panels) views of galaxies: g8.26e11, g1.12e12, g1.77e12, g2.79e12 after processing through the Monte Carlo radiative transfer code SUNRISE. Images are 50 kpc on a side.

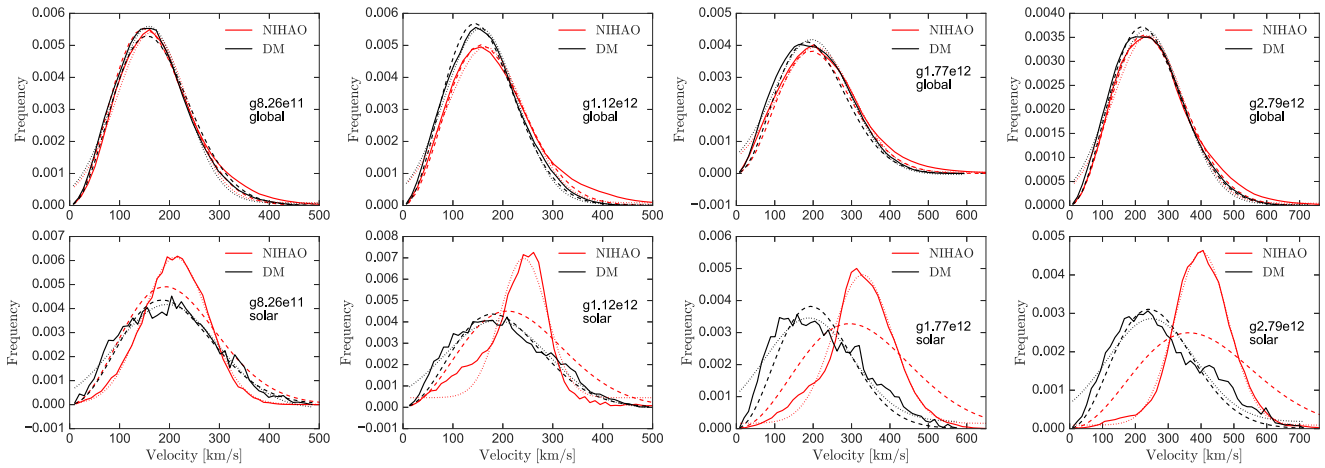

Figure 16. The dark matter particles velocity distribution in four additional galaxies with stellar and DM masses similar to the Milky Way: g8.26e11, g1.12e12, g1.77e12, g2.79e12. Symbols and lines are the same as in Fig. 14.

& Wechsler (2014) and Pillepich et al. (2014) for a more thorough discussion.

4 CONCLUSIONS

We used the NIHAO simulation suite (Wang et al. 2015) to investigate the impact of galaxy formation on the properties of the DM distribution within haloes.

The NIHAO suite is a large simulation campaign aiming to produce a large sample of high-resolution simulated galaxies in a cosmological context. It is an extension of the MaGICC simulations (Stinson et al. 2013) and it has been performed with an improved version of the SPH GASOLINE code (Keller et al. 2014) which fixes the well-known problems of particle-based hydrodynamical codes (Agertz et al. 2007). The NIHAO project counts more than 90 simulated galaxies across two orders of magnitude in halo mass (10^{10}–10^{12} $M_{\odot}$), with each of the galaxies resolved with at least 4×10^5 elements.

The NIHAO galaxies have been very successful in reproducing stellar to halo mass ratio on more than five orders of magnitude in stellar mass: from 10^5 to 10^{11} $M_{\odot}$. They also show very realistic star formation histories for their stellar and halo masses. Finally, NIHAO galaxies are also consistent with the observed gas content of galaxy discs and haloes (Stinson et al. 2015; Wang et al. 2016; Gutcke et al. 2016). Thanks to the unprecedented combination of high-resolution and large statistical sample, the NIHAO suite offers a unique set of objects to study the distribution response of several DM properties to galaxy formation. Moreover, since for each galaxy we have, at the same resolution, an *N*-body-only (collisionless) simulation and

Table 3. Parameters describing the velocity distribution function at the virial radius (first two rows) and at the solar radius (second two rows) for the five Milky Way-like galaxies.

g8.26e11	m_1	m_2	g_1	μ	σ
$R_{\rm vir}$ (dm)	0.789	109.5	0.0055	158.9	70.42
$R_{\rm vir}$ (hydro)	0.794	105.7	0.0053	164.3	70.86
$R_\odot$ (dm)	0.776	131.0	0.0044	195.2	103.37
$R_\odot$ (hydro)	0.903	135.5	0.0061	211.8	64.69
g1.12e12	m_1	m_2	g_1	μ	σ
$R_{\rm vir}$ (dm)	0.787	101.9	0.0055	155.6	72.28
$R_{\rm vir}$ (hydro)	0.755	110.7	0.0049	165.0	76.96
$R_\odot$ (dm)	0.754	127.0	0.0041	187.3	104.2
$R_\odot$ (hydro)	0.905	147.7	0.0066	241.9	46.79
g1.77e12	m_1	m_2	g_1	μ	σ
$R_{\rm vir}$ (dm)	0.725	129.8	0.0042	195.5	99.00
$R_{\rm vir}$ (hydro)	0.713	137.0	0.0039	206.6	99.80
$R_\odot$ (dm)	0.712	137.1	0.0032	189.2	115.22
$R_\odot$ (hydro)	0.929	208.3	0.0047	328.7	76.69
g1.92e12	m_1	m_2	g_1	μ	σ
$R_{\rm vir}$ (dm)	0.739	144.5	0.0035	211.6	122.3
$R_{\rm vir}$ (hydro)	0.699	140.37	0.0033	203.6	119.5
$R_\odot$ (dm)	0.735	159.5	0.0030	232.0	115.2
$R_\odot$ (hydro)	0.969	218.0	0.0058	348.1	60.49
g2.79e12	m_1	m_2	g_1	μ	σ
$R_{\rm vir}$ (dm)	0.783	155.0	0.0036	231.9	110.0
$R_{\rm vir}$ (hydro)	0.774	160.1	0.0035	239.4	109.2
$R_\odot$ (dm)	0.722	170.9	0.0027	249.0	133.8
$R_\odot$ (hydro)	0.870	256.6	0.0045	401.5	81.91

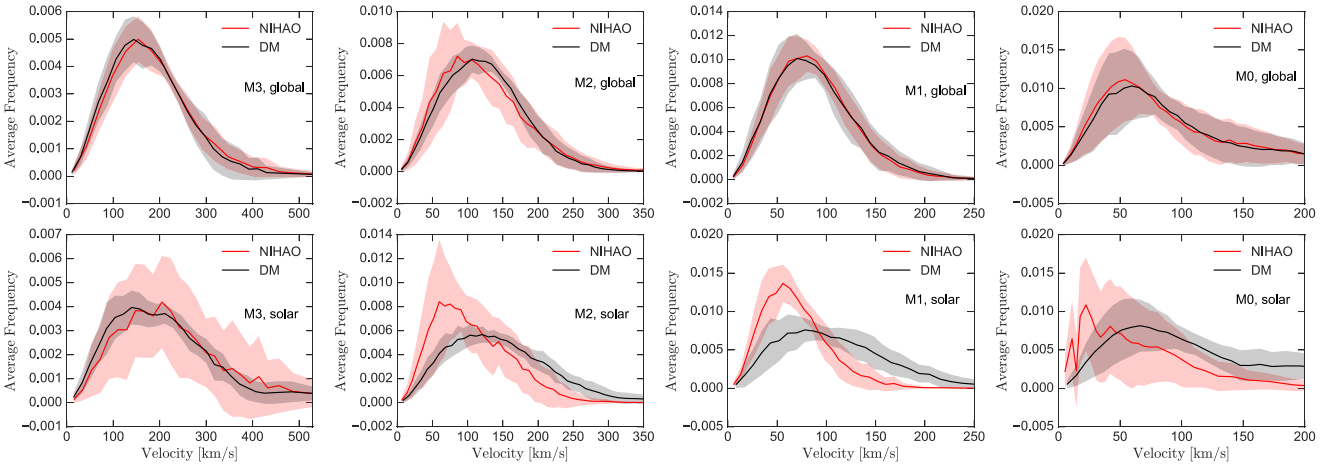

Figure 17. Same as Fig. 14 but averaged in the four mass bins M0–M3 (M0 < M1 < M2 < M3 $\sim 10^{12}\,M_\odot$).

a full hydrodynamical simulation, we are able to assess the effect of baryons on a halo-by-halo basis.

In this study, we focused on three key properties of DM haloes: the halo shape, the radial profile of the pseudo phase-space density and the DM velocity distribution both global and in the solar neighbourhood. Our results can be summarized as follows.

(i) The shape of the DM halo within the virial radius is similar between DM-only and hydro simulations. At smaller radii, however, the hydro simulations become rounder. There is a strong mass dependence to the difference between the inner halo shape (measured at 12 per cent of the virial radius) from the DM-only simulations and hydro simulations. At low masses, ($<10^{11}\,M_\odot$) the DM halo tends to retain its original triaxial shape, while at higher masses ($\approx 10^{12}\,M_\odot$), the inner halo becomes more spherical with an average minor to major axis ratio (c/a) of 0.8. This brings numerical predictions into good agreement with estimates of the inner halo shape in our own Galaxy. We show that the mass dependence of the variation of the halo shape is related to the increase of star formation efficiency with halo mass, which raises the contribution of stars and gas to the overall potential.

We provide a simple fitting formula that relates the change in the axis ratio c/a with the ratio between stellar mass and halo mass, and in principle, allows the prediction of the shape of a galaxy DM halo from its stellar and dynamical mass.

(ii) In hydrodynamical simulations, the radial behaviour of the DM pseudo phase-space density $Q \equiv \rho/\sigma^3$ is not always well represented by a single power law. At total masses $M \gtrsim 10^{11}$ M$_\odot$, the Q radial profile shows a flattening towards the centre of the halo. This is related to the change in the DM density profile which strongly departs from the pure DM results in the NIHAO simulations (Tollet et al. 2016). Overall, hydro simulations have a lower value of Q compared to the N-body case, when it is measured at a fix fraction of the virial radius.

(iii) The velocity distribution of the DM particles within the virial radius in the hydro simulations is still well represented by a Maxwellian distribution, and it is similar to the DM-only case at all mass scales.

When we restrict our analysis to the solar neighbourhood (7 kpc $< r <$ 9 kpc), we find that in the hydro simulations, the velocity distribution functional form strongly depends on the halo mass.

At low halo masses ($M \sim 10^{10}$ M$_\odot$, the hydro and DM-only simulations show a similar behaviour, when we move to higher masses ($M \sim 10^{11}$ M$_\odot$), the velocity distribution becomes progressively more symmetric and the velocity peak moves towards lower values with respect to the N-body case, then in our most massive bin ($M \sim 10^{11}$ M$_\odot$), the distribution is again in agreement with the N-body case. We tentatively ascribed this trend to the different reaction of the DM distribution as function of increasing halo mass from few 10^9 M$_\odot$ to M>10^{12} M$_\odot$ (namely no effect, halo expansion, no effect and halo contraction) as described in details in Tollet et al. (2016) and Dutton et al. (2016a).

To better study this effect, we isolated five galaxies that, for stellar and total mass, resemble our own Milky Way. For these galaxies, the maximum of the velocity distribution in the hydro simulations moves to higher velocities with respect to the N-body case, due to an overall halo contraction in these galaxies, and we find very little correlation with the galaxy morphology. In our Milky Way analogues, the velocity distribution is well fitted by a Gaussian and we provide the fitting parameters of the distribution for five different galaxies. We also stress that the lack of high-velocity particles has important consequences for the interpretation and comparison of DM direct detection experiments.

Our results show that baryons have important effects on the DM not only in the very inner part (e.g. leading to expansion and contraction), but also on the global properties of DM. The understanding of the nature of DM and the comparison of theoretical predictions with observational data can no longer rely on pure collisionless simulations, but must include the effects of visible matter.

ACKNOWLEDGEMENTS

We thanks an anonymous referee whose comments strongly improved the presentation of our results. The simulations were performed on the THEO cluster of the Max Planck Institute for Astronomy, and HYDRA cluster, both based at the Rechenzentrum in Garching, and on the High Performance Computing resources at New York University Abu Dhabi. AVM, AAD, and GSS acknowledge support from the Sonderforschungsbereich SFB 881 'The Milky Way System' (subproject A1) of the German Research Foundation (DFG). IB contribution to this project was made possible through the SURF program at Caltech, and was supported by the Flintridge Foundation, Caltech SFP Office, and Christian Ott. IB also acknowledges support from the Sonderforschungsbereich SFB 881 'The Milky Way System' (subproject A1) of the German Research Foundation (DFG) during her stay at the MPIA. XK acknowledge the support from NSFC project No.11333008. CP is supported by funding made available by ERC-StG/EDECS n. 279954. Finally, IB would like to thank Lynne Hillenbrand for her guidance in writing this paper.

REFERENCES

Abadi M. G., Navarro J. F., Fardal M., Babul A., Steinmetz M., 2010, MNRAS, 407, 435
Agertz O. et al., 2007, MNRAS, 380, 963
Agnese R. et al., 2013, Phys. Rev. Lett., 111, 251301
Allgood B., Flores R. A., Primack J. R., Kravtsov A. V., Wechsler R. H., Faltenbacher A., Bullock J. S., 2006, MNRAS, 367, 1781
Aprile E. et al., 2012, Phys. Rev. Lett., 109, 181301
Austin C. G., Williams L. L. R., Barnes E. I., Babul A., Dalcanton J. J., 2005, ApJ, 634, 756
Bertschinger E., 2001, ApJS, 137, 1
Bett P., Eke V., Frenk C. S., Jenkins A., Helly J., Navarro J., 2007, MNRAS, 376, 215
Bryan S. E., Kay S. T., Duffy A. R., Schaye J., Dalla Vecchia C., Booth C. M., 2013, MNRAS, 429, 3316
Chabrier G., 2003, PASP, 115, 763
Debattista V. P., Moore B., Quinn T., Kazantzidis S., Maas R., Mayer L., Read J., Stadel J., 2008, ApJ, 681, 1076
Dehnen W., Binney J., 1998, MNRAS, 294, 429
Dehnen W., McLaughlin D. E., 2005, MNRAS, 363, 1057
Di Cintio A., Brook C. B., Macciò A. V., Stinson G. S., Knebe A., Dutton A. A., Wadsley J., 2014a, MNRAS, 437, 415
Di Cintio A., Brook C. B., Dutton A. A., Macciò A. V., Stinson G. S., Knebe A., 2014b, MNRAS, 441, 2986
Dubinski J., 1994, ApJ, 431, 617
Dutton A. A., Macciò A. V., 2014, MNRAS, 441, 3359
Dutton A. A., Macciò A. V., Stinson G. S., Gutcke T. A., Penzo C., Buck T., 2015, MNRAS, 453, 2447
Dutton A. A. et al., 2016a, preprint (arXiv:1605.05323)
Dutton A. A., Macciò A. V., Frings J., Wang L., Stinson G. S., Penzo C., Kang X., 2016b, MNRAS, 457, L74
Gnedin O. Y., Kravtsov A. V., Klypin A. A., Nagai D., 2004, ApJ, 616, 16
Governato F. et al., 2010, Nature, 463, 203
Guedes J., Callegari S., Madau P., Mayer L., 2011, ApJ, 742, 76
Gutcke T. A., Stinson G. S., Macciò A. V., Wang L., Dutton A. A., 2016, preprint (arXiv:1602.06956)
Hayashi E., Navarro J. F., 2006, MNRAS, 373, 1117
Hayashi E., Navarro J. F., Springel V., 2007, MNRAS, 377, 50
Helmi A., 2004, ApJ, 610, L97
Ibata R., Lewis G. F., Irwin M., Totten E., Quinn T., 2001, ApJ, 551, 294
Jing Y. P., Suto Y., 2002, ApJ, 574, 538
Jonsson P., 2006, MNRAS, 372, 2
Katz N., Gunn J. E., 1991, ApJ, 377, 365
Kazantzidis S., Kravtsov A. V., Zentner A. R., Allgood B., Nagai D., Moore B., 2004, ApJ, 611, L73
Kazantzidis S., Abadi M. G., Navarro J. F., 2010, ApJ, 720, L62
Keller B. W., Wadsley J., Benincasa S. M., Couchman H. M. P., 2014, MNRAS, 442, 3013
Knollmann S. R., Knebe A., 2011, Astrophysics Source Code Library, record ascl:1102.009
Kuhlen M., Weiner N., Diemand J., Madau P., Moore B., Potter D., Stadel J., Zemp M., 2010, J. Cosmol. Astropart. Phys., 2, 30
Kuzio de Naray R., Kaufmann T., 2011, MNRAS, 414, 3617
Law D. R., Majewski S. R., 2010, ApJ, 714, 229
Lupton R., Blanton M. R., Fekete G., Hogg D. W., O'Mullane W., Szalay A., Wherry N., 2004, PASP, 116, 133

Macciò A. V., Dutton A. A., van den Bosch F. C., Moore B., Potter D., Stadel J., 2007, MNRAS, 378, 55
Macciò A. V., Dutton A. A., van den Bosch F. C., 2008, MNRAS, 391, 1940
Macciò A. V., Stinson G., Brook C. B., Wadsley J., Couchman H. M. P., Shen S., Gibson B. K., Quinn T., 2012, ApJ, 744, L9
Mao Y.-Y., Strigari L. E., Wechsler R. H., 2014, Phy. Rev. D, 89, 063513
Martínez-Delgado D., Gómez-Flechoso M. Á., Aparicio A., Carrera R., 2004, ApJ, 601, 242
Mashchenko S., Couchman H. M. P., Wadsley J., 2006, Nature, 442, 539
Merritt D., Navarro J. F., Ludlow A., Jenkins A., 2005, ApJ, 624, L85
Moster B. P., Somerville R. S., Maulbetsch C., van den Bosch F. C., Macciò A. V., Naab T., Oser L., 2010, ApJ, 710, 903
Navarro J. F. et al., 2004, MNRAS, 349, 1039
Neto A. F. et al., 2007, MNRAS, 381, 1450
Obreja A., Stinson G. S., Dutton A. A., Macciò A. V., Wang L., Kang X., 2016, MNRAS, 459, 467
Oh S.-H. et al., 2015, AJ, 149, 180
Oñorbe J., Boylan-Kolchin M., Bullock J. S., Hopkins P. F., Kereš D., Faucher-Giguère C.-A., Quataert E., Murray N., 2015, MNRAS, 454, 2092
Pedrosa S., Tissera P. B., Scannapieco C., 2009, MNRAS, 395, L57
Penzo C., Macciò A. V., Casarini L., Stinson G. S., Wadsley J., 2014, MNRAS, 442, 176
Pillepich A., Kuhlen M., Guedes J., Madau P., 2014, ApJ, 784, 161
Planck Collaboration XVI, 2014, A&A, 571, A16
Pontzen A., Governato F., 2012, MNRAS, 421, 3464
Ritchie B. W., Thomas P. A., 2001, MNRAS, 323, 743
Saitoh T. R., Makino J., 2009, ApJ, 697, L99
Schaye J. et al., 2010, MNRAS, 402, 1536
Schmidt K. B., Hansen S. H., Macciò A. V., 2008, ApJ, 689, L33
Shen S., Wadsley J., Stinson G., 2010, MNRAS, 407, 1581
Springel V., White S. D. M., Hernquist L., 2004, in Ryder S., Pisano D., Walker M., Freeman K., eds, Proc. IAU Symp. 220, Dark Matter in Galaxies. Kluwer, Dordrecht, p. 421
Stadel J. G., 2001, PhD thesis, Univ. Washington
Stinson G., Seth A., Katz N., Wadsley J., Governato F., Quinn T., 2006, MNRAS, 373, 1074
Stinson G. S., Stadel J., Maccio A., Wadsley T., Quinn T. H. M. P. C., 2013, MNRAS, 428, 129
Stinson G. S. et al., 2015, MNRAS, 454, 1105
Taylor J. E., Navarro J. F., 2001, ApJ, 563, 483
Teyssier M., Johnston K. V., Kuhlen M., 2012, MNRAS, 426, 1808
Tissera P. B., White S. D. M., Pedrosa S., Scannapieco C., 2010, MNRAS, 406, 922
Tollet E. et al., 2016, MNRAS, 456, 3542
Vergados J. D., Hansen S. H., Host O., 2008, Phy. Rev. D, 77, 023509
Vogelsberger M. et al., 2009, MNRAS, 395, 797
Wadsley J. W., Stadel J., Quinn T., 2004, New Astron., 9, 137
Wadsley J. W., Veeravalli G., Couchman H. M. P., 2008, MNRAS, 387, 427
Wang L., Dutton A. A., Stinson G. S., Macciò A. V., Penzo C., Kang X., Keller B. W., Wadsley J., 2015, MNRAS, 454, 83
Wang L., Dutton A. A., Stinson G. S., Macciò A. V., Gutcke T., Kang X., 2016, preprint (arXiv:1601.00967)

This paper has been typeset from a TEX/LATEX file prepared by the author.